American Mineralogist, Volume 75, pages 392–397, 1990

Chromium incorporation in mullite

H. Rager
Fachbereich Geowissenschaften der Universität, Lahnberge, D-3550 Marburg, FRG
H. Schneider
Forschungsinstitut der Feuerfest-Industrie, An der Elisabethkirche 27, D-5300 Bonn 1, FRG
H. Graetsch
Institut für Mineralogie, Ruhr-Universität Bochum, D-4630 Bochum 1, FRG

Abstract

Mullites with Cr contents up to about 12 wt% (6.5 mol%) Cr_2O_3 and with Cr plus Fe contents up to about 8 wt% (4.5 mol%) Cr_2O_3 and 8 wt% (4.5 mol%) Fe_2O_3 were synthesized from oxide powder mixtures by means of solid-state sintering. Microchemical analyses, X-ray powder diffractometry, and electron paramagnetic resonance spectroscopy were used to characterize the structural mechanisms of Cr and Cr plus Fe doping. The studies yielded evidence for substitution of Cr^{3+} for Al^{3+} in the $Al(1)O_6$ octahedra of the structure and for Cr^{3+} incorporation at octahedrally coordinated interstices, respectively. Although the solubility of trivalent cations in mullite generally is limited to about 6.5 oxide mol%, Cr-rich mullites annealed with Fe-rich silicate melts contain up to about 9 mol% $(Cr,Fe)_2O_3$. This extension of the substitution limit is explained by part of the Cr^{3+} ions entering interstitial sites, leaving space for Fe^{3+} to enter the octahedra.

Introduction

Mullite is an aluminum silicate with the general composition $Al_{4+2x}Si_{2-2x}O_{10-x}$ ($0 \leq x \leq 1$, Cameron, 1977). The orthorhombic crystal structure of mullite is very similar to that of sillimanite (Burnham, 1963) in that it has chains of edge-sharing $Al(1)O_6$ octahedra [nomenclature used throughout the paper is that of Burnham (1964)] parallel to the crystallographic *c* axis. Octahedral columns are crosslinked by double chains of $Al(2)O_4$ and SiO_4 tetrahedra, which are also parallel to *c*. As a result of the higher Al content of mullite relative to sillimanite, some O atoms bridging adjacent tetrahedra are removed to maintain charge neutrality. As a consequence, a new tetrahedral site is occupied in which the bridging O atoms belong to three tetrahedra (e.g., Burnham, 1964; Saalfeld and Guse, 1981; Angel and Prewitt, 1986). The reduction of the *c* lattice parameter of mullite (≈2.9 Å) to half of the value of *c* in sillimanite (≈5.8 Å) and the mean tetrahedral T-O distance in 3:2 mullite (1.69 Å, Saalfeld and Guse, 1981), which lies between the tetrahedral Si-O (1.60 Å) and Al-O (1.76 Å) distances of sillimanite (Burnham, 1963), indicate a random distribution of tetrahedral Al and Si in mullite, instead of an ordered Al/Si distribution in sillimanite. This is confirmed by infrared spectra and by the thermochemical calculations of Holm and Kleppa (1966).

Depending on the synthesis procedure, the mullite structure is able to incorporate considerable amounts of impurities. Of special importance are the transition metal cations Ti^{3+}, Ti^{4+}, V^{3+}, V^{4+}, V^{5+}, Cr^{3+}, Mn^{2+}, Mn^{3+}, Fe^{2+}, Fe^{3+}, and Co^{2+} (Schneider, 1986, 1989). There is evidence that the transition metals preferably enter the $Al(1)O_6$ octahedra, substituting for Al^{3+}. Fe^{3+} is also incorporated into the $Al(2)O_4$ tetrahedra, although in very small amounts (Schneider and Rager, 1986). Incorporation of Mn^{3+} into the $Al(1)O_6$ octahedra causes a strong deformation of the structure owing to Jahn-Teller distortion (Schneider and Vasudevan, 1989). The structural distribution of Cr^{3+} in mullite is of special interest because the low thermal expansion of mullite can be further reduced by Cr incorporation (Schneider and Eberhard, unpublished results). Understanding Cr incorporation could help to improve the behavior of mullite ceramics against sudden changes in temperature.

Experimental procedure

Bulk chemical analyses of the mullite samples were performed with a computer-controlled sequential spectrometer (XFA). Microanalyses (EMA) were carried out on polished sections with a computer-controlled Cameca CAMEBAX microprobe equipped with three wavelength-dispersive spectrometers. The resolution in the secondary electron picture was about 50 nm (measurement conditions: 15 kV, 30 mA). Quartz, corundum, and Cr_2O_3 were used as reference standards. To discriminate between mechanical inclusion and structural incorporation of Cr and Fe, only inclusion-free crystals were analyzed.

The X-ray powder-diffraction studies (XRD) were carried out at room temperature with a computer-controlled Siemens D-500 powder diffractometer (Cu$K\alpha$ radiation, secondary graphite monochromator, variable aperture

0003–004X/90/0304–0392$02.00

TABLE 1. Chemical composition and cell parameters of Cr- and Cr-Fe–doped mullites

Sample key		Chemical composition Al_2O_3 (wt%)	SiO_2 (wt%)	Cr_2O_3 (wt%)	Fe_2O_3 (wt%)	x	Cell parameters a (Å)	b (Å)	c (Å)	V (Å)³
Cr-doped mullites										
Cr 0	a	71.2(2)	28.6(2)		—					
	b	71.3	28.6	—	—	0.24	7.5454(2)	7.6908(2)	2.8829(1)	167.294(6)
Cr 0.25	a	n.d.	n.d.	—						
	b	71.5	28.2	0.26	—	0.25	7.5459(2)	7.6909(2)	2.8831(1)	167.323(4)
Cr 0.5	a	70.1(5)	29.3(5)	0.57(2)	—					
	b	70.9	28.5	0.60	—	0.24	7.5457(4)	7.6908(4)	2.8835(2)	167.34(1)
Cr 1	a	n.d.	n.d.	n.d.	—					
	b	70.5	28.4	1.10	—	0.24	7.5477(3)	7.6922(4)	2.8846(2)	167.479(9)
Cr 2	a	68.8(3)	28.9(4)	2.3(2)	—					
	b	69.0	28.7	2.30	—	0.23	7.5498(5)	7.6951(7)	2.8867(2)	167.71(1)
Cr 3.5	a	67.3(4)	28.5(3)	4.1(2)	—					
	b	68.0	28.3	3.70	—	0.24	7.5523(2)	7.6965(2)	2.8891(1)	167.93(5)
Cr 5	a	65.7(4)	28.5(4)	5.7(2)	—					
	b	66.4	28.0	5.60	—	0.24	7.5561(2)	7.7006(2)	2.8921(1)	168.281(5)
Cr 6	a	64.1(2)	28.5(2)	7.3(2)	—					
	b	65.6	28.0	6.40	—	0.24	7.5580(2)	7.7018(3)	2.8937(1)	168.445(6)
Cr 7.5	a	62.8(4)	28.4(3)	8.6(2)	—					
	b	64.2	27.7	8.10	—	0.24	7.5624(4)	7.7067(5)	2.8973(2)	168.861(1)
Cr 8.5	a	61.7(4)	28.3(2)	9.9(3)	—					
	b	62.9	27.9	9.20	—	0.23	7.5643(4)	7.7065(5)	2.8985(2)	168.966(2)
Cr 10	a	60.0(4)	28.4(3)	11.5(2)	—					
	b	61.9	27.8	10.3	—	0.23	7.5674(5)	7.7089(7)	2.9010(2)	169.23(2)
Cr 12.5	a	59.2(8)	28.9(8)	12.0(5)	—					
	b	n.d.	n.d.	n.d.	—	n.d.	7.5685(5)	7.7105(6)	2.9019(2)	169.35(1)
Cr-Fe–doped mullites										
Cr 5/Fe 1	b	64.6	28.5	5.55	1.32	0.22	7.5574(3)	7.7021(3)	2.8937(2)	168.44(1)
Cr 5/Fe 2.5	b	63.8	28.3	5.24	2.58	0.23	7.5603(5)	7.7060(6)	2.8948(3)	168.65(2)
Cr 5/Fe 5	b	62.7	28.0	4.30	4.97	0.23	7.5659(4)	7.7137(5)	2.8970(2)	169.07(1)
Cr 5/Fe 7.5	b	61.9	28.1	4.18	5.72	0.22	7.5681(7)	7.7157(7)	2.8976(3)	169.20(2)
Cr 10/12.5 L-Fe	b	59.8	27.8	8.80	3.68	0.23	7.5704(8)	7.7170(9)	2.9037(5)	169.64(3)
Cr 10/25 L-Fe	b	57.1	27.5	7.71	7.74	0.23	7.5762(5)	7.7280(5)	2.9059(2)	170.13(2)

Note: Values in parentheses are standard deviations. x = Structural state of mullite, referring to the general formula $M_{4+2x}Si_{2-2x}O_{10x}$ ($M = Al^{3+}, Cr^{3+}, Fe^{3+}$). n.d. = not determined. a = microprobe analyses, b = X-ray fluorescence analyses.

slit). The diffractograms were recorded in the range 5 to 75° 2θ in step-scan mode (5 s per 0.01° 2θ). Si (a = 5.43088(4) Å) was used as an internal standard. Integrated intensities, full width at half maximum, and d values were evaluated with a least-squares-fit program using Pseudo-Voigt functions. Lattice constants were refined with a least-squares procedure using 20 medium and strong reflections in the range 20 to 70° 2θ.

The electron paramagnetic resonance (EPR) spectra were measured from about 40 mg of the powdered samples at X-band frequency with a Varian spectrometer using 100 kHz modulation. The temperature dependence of the spectra was studied in the temperature range between 4 and 290 K. The observed EPR signals are represented by their effective g values (g_{eff}) defined by $h\nu = g_{eff}\beta B$, where B is the external magnetic field at which the EPR signal appears, ν is the microwave frequency used, β is the Bohr magneton, and h is the Planck constant. The frequency was determined by an HP 5340 frequency counter, and the magnetic field scale was calibrated using the proton magnetic resonance of H_2O. The area under the integrated EPR signals was used as a measure of their intensities.

SAMPLE MATERIAL

Each mullite composition was made from about 4 g of chemically pure Al_2O_3 (VAW, 302), SiO_2 (Ventron, 88316), Cr_2O_3 (Merck, 2483), and Fe_2O_3 (Riedel de Haen, 12344) powders, with $62 - (x + y)$ wt% Al_2O_3, 38 wt% SiO_2, x wt% Cr_2O_3 (x = 0, 0.25, 0.5, 1, 2, 3.5, 5.6, 7.5, 8.5, 10, 12.5; samples Cr 0 to Cr 12.5), and with 5 wt% Cr_2O_3 and y wt% Fe_2O_3 (y = 1, 2.5, 5, 7.5, samples Cr 5/Fe 1 to Cr 5/Fe 7.5) starting materials. The carefully homogenized powders had mean grain sizes of about 5 μm. The mixtures were pressed to 20 mm diameter × 5 mm height disks in a pressing mold using uniaxial pressure loading. All synthesis and annealing experiments were carried out in a laboratory furnace in air at 1 atm. To determine the best synthesis conditions, preliminary synthesis experiments were performed at 1400, 1500, 1600, and 1650 °C. The greatest amount of Cr incorporation occurred at 1650 °C. Consequently all Cr-doped mullite syntheses were carried out at this temperature. The sample disks containing Cr and Fe were prefired 12 h at 1450 °C to avoid Fe_2O_3 decomposition and then were annealed at 1650 and 1450 °C. Prior to the structural characterization of the mullites the annealed samples were washed with a HF-HCl acid solution to leach the coexisting glass phases.

Other Cr- and Fe-rich mullites were prepared by a multistep procedure in which a Cr 10 mullite was synthesized, treated with HF and HCl, mixed with 12.5 wt% (sample Cr 10/12.5-Fe) and 25 wt% of an Fe-rich silicate

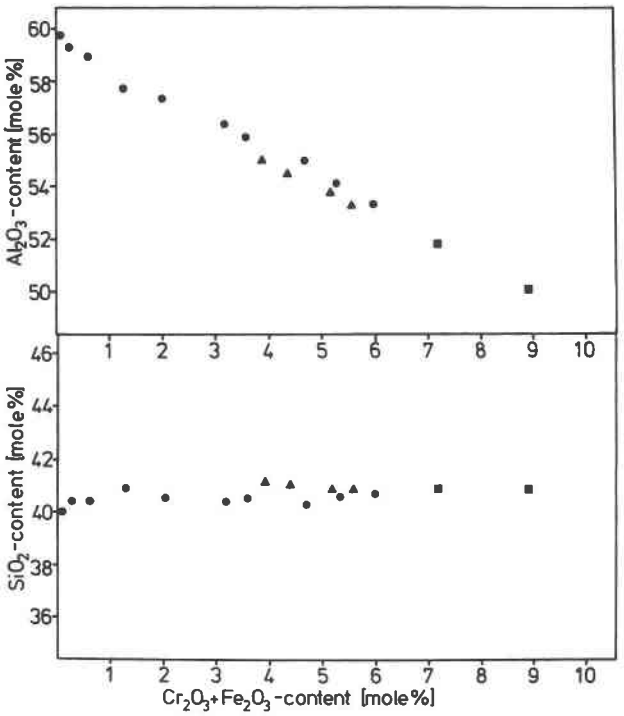

Fig. 1. Cr_2O_3 and Cr_2O_3 + Fe_2O_3 contents of mullite plotted versus Al_2O_3 and SiO_2. Circles: Cr-doped mullites (samples Cr 0 to Cr 10, Table 1). Triangles: Cr-Fe–doped mullite (samples Cr 5Fe1 to Cr 5Fe7.5, Table 1). Squares: Cr-doped mullites, annealed together with Fe-rich melts (samples Cr 10/25 L-Fe and Cr 10/12.5 L-Fe, Table 1).

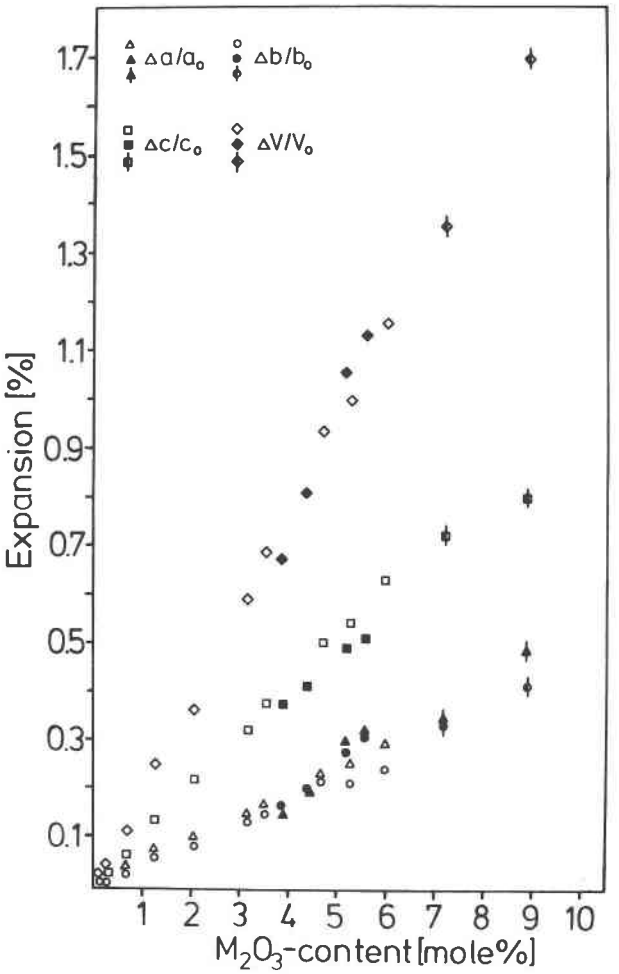

Fig. 2. Percentage structural expansion of Cr- and of Cr-Fe–doped mullites plotted versus transition metal oxide content of the phases. Open symbols: Cr-doped mullites (samples Cr 0 to Cr 10, Table 1). Filled symbols: Cr-Fe–doped mullites (samples Cr 5Fe1 to Cr 5Fe7.5, Table 1). Open symbols with bars: Cr-doped mullites annealed together with Fe-rich melts (samples Cr 10/25 L-Fe and Cr 10/12.5 L-Fe, Table 1).

glass (sample Cr 10/25 L-Fe), pressed to sample discs, and then annealed at 1400 °C. After the heat treatment the material was again washed with HF/HCl. The bulk chemical composition (in wt%) of sample Cr 10/12.5 L-Fe is Al_2O_3 54.5, SiO_2 33.3, Cr_2O_3 8.6, and Fe_2O_3 3.6. The composition of sample Cr 10/25 L-Fe is Al_2O_3 46, SiO_2 39, Cr_2O_3 7, and Fe_2O_3 8.

Results

The heat treatment of the Cr-containing powder pellets produced mullite crystals up to about 20 μm in diameter. The crystals display reniform surfaces and are embedded in a coexisting silicate glass. The Cr- and Fe-containing mullites have larger grain sizes, up to about 100 μm, and the shape of the crystals is tabular or acicular.

Cr-rich mullite samples are green, whereas Cr-Fe–rich materials have colors varying between greenish (Cr-rich) and brownish (Fe-rich). Chemical analyses of HF-HCl–treated bulk samples obtained by XFA and of Cr-doped mullites obtained by EMA are in Table 1. The mullites contain up to about 12 wt% Cr_2O_3 and 15 wt% Cr_2O_3 + Fe_2O_3, respectively. The Cr_2O_3 and Cr_2O_3 + Fe_2O_3 contents of the untreated bulk samples correlate with those of mullite, indicating that the Cr and Cr-Fe distribution coefficients between mullite and the coexisting glass phase are independent of the transition metal content of the starting materials. A reciprocal equimolar dependence exists between Cr_2O_3 and Al_2O_3, and between Cr_2O_3 + Fe_2O_3 and Al_2O_3 (Fig. 1). The structural formula of the Cr- and Cr-Fe–substituted mullites (Table 1) is very close to that of 3:2 mullite ($3Al_2O_3 \cdot 2SiO_2$) in each case.

X-ray powder diffractometer studies show that the samples investigated are single phase mullite, except sample Cr 12.5, for which weak additional X-ray reflections indicate the presence of a small amount of $(Al,Cr)_2O_3$. The half widths of the reflections are only slightly broadened with increasing Cr and Cr-Fe substitution. Cr incorporation causes a linear increase of the cell parameters (Fig. 2). The expansion is greatest along the c-axis direction ($\Delta c/c$ = 0.11% per mole Cr_2O_3), followed by expansions along the a- and b-axis directions ($\Delta a/a$ = 0.05%,

and $\Delta b/b = 0.04\%$ per mole percent Cr_2O_3). Simultaneous Cr and Fe incorporation into mullite produces a cell-volume expansion that lies on the straight line of Cr-doped mullites (Fig. 2).

Electron paramagnetic resonance (EPR) measurements of all Cr-doped mullites with Cr_2O_3 contents up to about 8.5 wt% reveal qualitatively the same patterns (Figs. 3a, b). The EPR spectra consist of two rather sharp signals near $g_{eff} = 5$ and a broad EPR signal that crosses the base line near $B = 3000$ G. The broad signal exhibits a fine structure with shoulders below and above $g_{eff} = 2.2$. With increasing Cr content the two sharp EPR signals broaden and decrease in intensity, and the fine structure of the broad signal disappears. Simultaneously, the overall intensity of the EPR patterns increases and the baseline crossover of the broad signal is shifted toward higher magnetic fields. Decreasing temperature does not cause a significant change in the EPR patterns. Mullites containing more than about 8.5 wt% Cr_2O_3 (Table 1) exhibit an additional EPR signal at $g_{eff} = 1.98$ with a line width of about 350 G and a symmetric Lorentzian line shape. At temperatures slightly higher than 25 °C the signals' intensity rapidly increases, which is indicative of antiferromagnetically coupled Cr^{3+}, as in crystalline Cr_2O_3 (Dräger and Gerling, 1981). The occurrence of Cr_2O_3 inclusions in mullites with Cr_2O_3 contents above 8.5 wt% (sample Cr 10, Table 1) but not in samples with lower Cr content has been observed by analyzing Cr-doped mullites with transmission electron microscopy (Ashworth and Schneider, unpublished results). In addition most of our EPR spectra contain a weak signal near $g_{eff} = 4.2$, which we attribute to the presence of a trace amount of Fe^{3+}.

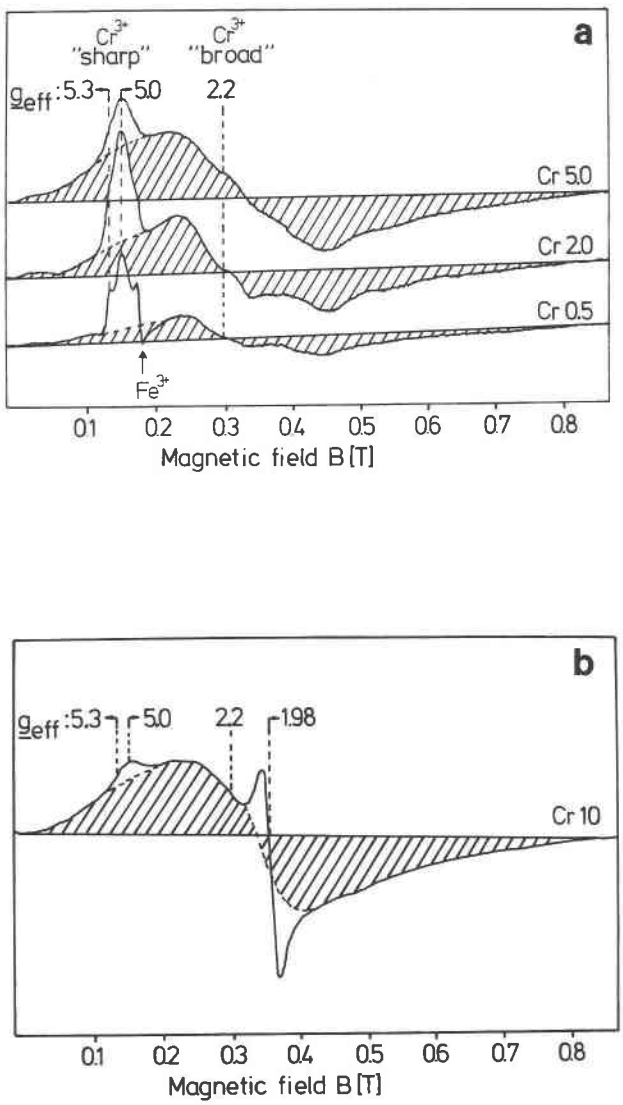

Fig. 3. EPR spectra of Cr-doped mullites Cr 0.5, Cr 2, and Cr 5 (**a**), and of Cr 10 (**b**) (Table 1). The spectra were taken at 9.518 GHz and room temperature, using 1 mW microwave power and 5.10^{-4} T modulation amplitude at 100 kHz modulation frequency. The hatched areas of Figs. 3a and 3b correspond to the EPR signal denoted by $g_{eff} = 2.2$.

Discussion

Because of the direct correspondence between the shape of the EPR patterns and the Cr content in mullite, we assume that the EPR signals are due to the occurrence of Cr^{3+} in the structure.

The EPR spectra of powders containing Cr^{3+} are difficult to interpret. Barry (1969) pointed out that in strong crystal fields, where the zero-field splitting exceeds the energy of the microwave, the Cr^{3+} EPR spectrum is dominated by a peak at $g_{eff} = 3.8$ in the case of a uniaxial crystal field symmetry and by a signal at $g_{eff} = 5.4$ for an orthorhombic field. Calculation of the g-values for the effective Cr^{3+}-spin S = 3/2 (Hutton, 1969) yields a splitting of the EPR signal at $g_{eff} = 5.4$ into two components, when the crystal field changes from orthorhombic to uniaxial symmetry. In the splitting, one component shifts toward lower and the other toward higher g_{eff} values. Applied to EPR spectra of Cr^{3+}-doped mullite, this result means that the two sharp peaks near $g_{eff} = 5$ should be assigned to Cr^{3+} in a strong crystal field of orthorhombic character. Le Marshall et al. (1971), studying the Cr^{3+}-distribution in sillimanite by EPR, gave evidence for a strong orthorhombic crystal field for the Cr^{3+} center located in a slightly distorted octahedral environment. The similarity of the crystal structures of sillimanite and mullite and the preference of Cr^{3+} for octahedral sites allows the assignment of the sharp EPR peaks near $g_{eff} = 5$ to Cr^{3+} in slightly distorted octahedral Al(1) positions in mullite.

All Cr-doped mullites investigated exhibit a broad, slightly asymmetric EPR signal near $g_{eff} = 2.2$, the intensity of which depends on the Cr content. Asymmetric and broad microwave absorption of this type occurs in paramagnetic solids and is indicative of coupling between localized magnetic moments. Assignment of the broad band to coupled Cr ions would mean that Cr^{3+} may occur in pairs, in groups of several ions, or even in clusters. Assuming Cr incorporation in the $Al(1)O_6$ octahedra only, the occurrence of Cr^{3+} both in pairs or in groups of more

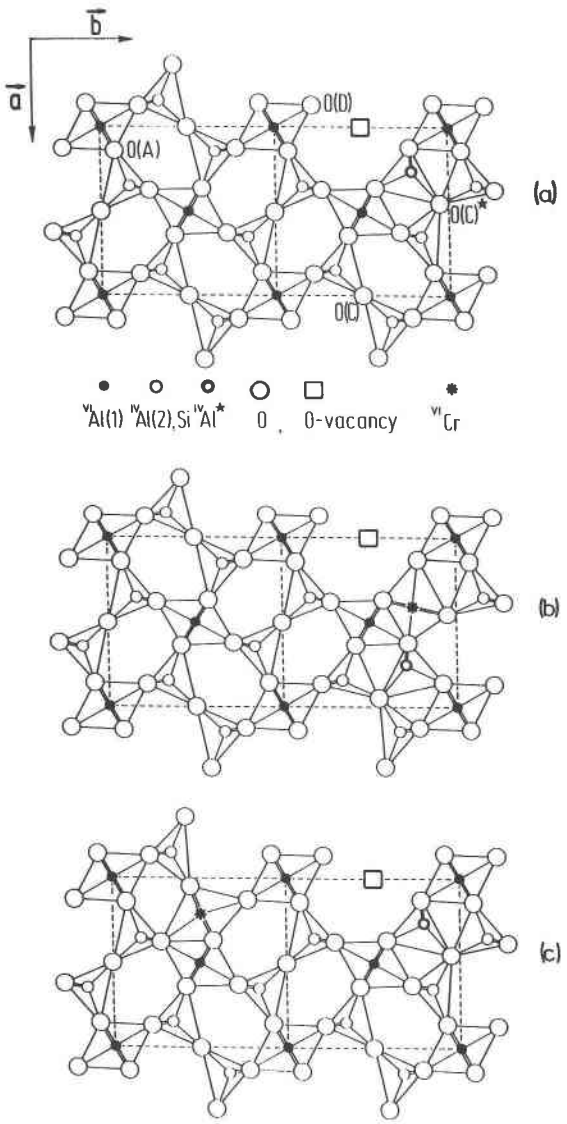

Fig. 4. Structural models for Cr^{3+} incorporation into mullite (a) Transition-metal–free mullite. (b) Substitution of $^{[6]}Cr^{3+}$ for $^{[4]}Al^{(*)3+}$ near the O vacancy. (c) Substitution $^{[6]}Cr^{3+}$ for $^{[4]}Al(2)^{3+}$ in the structural channel running parallel to *c*. The crystal structure of mullite is drawn in a projection down the *c* axis in each case.

than two ions seems to be not very probable, especially in mullites with low Cr contents. However, occurrence of pairs or groups of more than two ions becomes more reasonable if Cr incorporation in the $Al(1)O_6$ octahedra and in interstitial structural sites is taken into account. A similar idea was presented by Landry et al. (1967), who studied the EPR spectra of Cr-doped aluminophosphate glasses as a function of Cr_2O_3 concentration and likewise proposed Cr pairs with Cr at interstitial sites.

The strong preference of Cr^{3+} for octahedral coordination (Wells, 1984) suggests that interstitial Cr^{3+} could be located in distorted, interstitial octahedral environments. Such sites in mullite are (1) the structural vacancies formed by removal of O atoms [O(C)] that bridge adjacent tetrahedra near (0.1, 0.25, 0) (Fig. 4b) and (2) the relatively wide structural channels running along *c* near (0.2, 0.5, 0) (Fig. 4c). Possible octahedral sites in the O(C) vacancies are strongly distorted but become more regular if the O(C)* position is occupied. This is the case near the characteristic O vacancies of the mullite structure. Such sites become almost completely regular by a small additional O(C)* shift toward the center of the octahedron. Incorporation of Cr^{3+} on equipoint (4*g*) near (0.1, 0.25, 0) implies that the nearest $^{[4]}Al^*$ position cannot be occupied, which is equivalent to the substitution $^{[6]}Cr^{3+} \rightarrow {}^{[4]}Al^{(*)3+}$. In addition, adjacent $Al(2)O_4$ tetrahedra, which would share an edge with the new octahedron, must be vacant, or the Al(2)-ion must occupy an additional Al* site. Cr incorporation into the structural channels in a distorted octahedral environment near (0.2, 0.5, 0) does not require any severe changes in the configuration of adjacent polyhedra. It can be described by the substitution scheme $^{[6]}Cr^{3+} \rightarrow {}^{[4]}Al(2)^{3+}$. Both types of interstitial octahedra form pairs with the $Al(1)O_6$ octahedra by sharing common faces, as in the corundum structure. Furthermore, the proposed substitution schemes do not need any charge compensation mechanism. Therefore, we interpret the broad EPR signal at $g_{eff} \approx 2.2$ as being mainly due to Cr pairs, where the formation of pairs may occur via occupation of neighboring regular octhahedral sites, or through occupation of adjacent regular and interstitial sites, or both.

Because mullites containing Cr_2O_3 up to 8.5 wt% show qualitatively the same EPR pattern, it is possible to make a rough estimation of the Cr distribution over the different structure sites by using the ratio of the integrated EPR peaks near $g_{eff} = 5$ and of the broad signals near $g_{eff} = 2.2$. Given this assumption, entry of Cr^{3+} into the regular $Al(1)O_6$ octahedra is favored at low bulk Cr_2O_3 contents of mullite, whereas interstitial incorporation with formation of Cr clusters becomes more important at higher Cr_2O_3 contents (Fig. 3a).

Because the crystal structures of mullite and sillimanite are very similar (Burnham, 1963, 1964), the observation of Winter and Ghose (1979) that the thermal expansion of sillimanite is governed by the anisotropic expansion of the regular $Al(1)O_6$ octahedra may also explain the thermal expansion of mullite. In sillimanite the long Al(1)-O(D) distances increase more than the shorter Al(1)-O(A) and Al(1)-O(B) distances, resulting in a greater distortion of the octahedra at higher temperatures. The Al(1)-O(D) linkages are at an angle of only 30° with the *b* axis but at 60° to *a*, and as a consequence the *b* lattice constant expands more than *a*. This effect is further enhanced by a minor rotation of the polyhedra in such a way that Al(1)-O(D) bonds form a smaller angle with the *b* axis. This fact may also explain the expansion caused by substitution of large cations like Fe^{3+}, V^{3+}, and Ga^{3+} for Al^{3+} on octahedral sites (Schneider, 1989; Schneider and Rager, 1986) because of the geometrically analogous effects of

temperature and substitution on the crystal structure (Hazen, 1977). In contrast to the effect of Al^{3+} substitution by Fe^{3+}, V^{3+}, and Ga^{3+}, the entry of Cr^{3+} into mullite causes greater expansion along the *c* and *a* axes than along the *b* axis. This effect is probably due to the particular electronic configuration of Cr^{3+}, which not only causes the strong preference of Cr^{3+} for octahedral coordination but obviously also a preference for Cr-O distances of equal length (Trömel, 1983). Consequently, $^{[6]}Cr^{3+} \rightarrow {}^{[6]}Al(1)^{3+}$ substitution should not increase the distortion of the octahedra, especially the distortion along M(1)-O(D), to the same extent as substitution of $^{[6]}Fe^{3+}$, $^{[6]}V^{3+}$, and $^{[6]}Ga^{3+}$, which in turn may be responsible for the smaller *b* axis expansion of Cr-doped mullites. Incorporation of Cr^{3+} on interstitial octahedral sites may also hinder rotation of the long octahedral M(1)-O(D) bonds toward the *b* axis by constraining the face area shared by the $Al(1)O_6$ and interstitial octahedra.

Oxygen deficits in mullite can be examined using the *x*-values of the structural formula $M_{4+2x}Si_{2-2x}O_{10-x}$ with $M = Al^{3+}$, Cr^{3+}, Fe^{3+}. The *x*-values of the Cr- and Cr-Fe–doped mullites are very close to the one of 3:2 mullites, indicating comparable numbers of O vacancies and of Al* positions in the structures. The similar structural states of transition-metal–free and of Cr- and Cr-Fe–doped mullites are also documented by transmission electron microscopic analyses: transmission electron diffraction patterns of all mullites have the same type of diffuse satellite reflections, which indicate that the degree of ordering of O vacancies in the mullites is (nearly) independent of the transition metal distribution (Ashworth and Schneider, unpublished results).

Although the solubility of the trivalent cations V^{3+}, Fe^{3+}, and Ga^{3+} in mullite is limited to about 6.5 oxide mol% (Schneider, 1990), Cr-rich mullites annealed in contact with Fe-rich silicate melts contain up to about 9 mol% $(Cr,Fe)_2O_3$. This extension of the substitution limit is probably possible because part of the Cr^{3+} ions occupy interstitial sites, leaving space for Fe^{3+} to enter the octahedral chains parallel to *c*, until the concentration of Cr and Fe on the M(1) sites reaches a limit of 20% occupation by M^{3+} ions, which is comparable to the substitution limit of other trivalent cations.

Acknowledgments

We thank Mrs. H. Krause and Mrs. Chr. Buttgereit for their excellent technical assistance and Mrs. H. Vogel for typing the manuscript. The support of the Deutsche Forschungsgemeinschaft (DFG Bonn) for this research project is gratefully acknowledged.

References cited

Angel, R.J., and Prewitt, C.T. (1986) Crystal structure of mullite: A reexamination of the average structure. American Mineralogist, 71, 1476–1482.

Barry, T.I. (1969) Exploring the role of impurities in non-metallic materials by electron paramagnetic resonance. Journal of Material Science, 4, 485–498.

Burnham, C.W. (1963) Refinement of the crystal structure of sillimanite. Zeitschrift für Kristallographie, 115, 127–148.

——— (1964) Crystal structure of mullite. Carnegie Institution of Washington Year Book 63, 223–227.

Cameron, W.E. (1977) Mullite: A substituted alumina. American Mineralogist, 62, 747–755.

Dräger, K., and Gerling, R. (1981) Der Einfluß unmagnetischer Dotierungen auf die ESR-Linienbreite von antiferromagnetischen Verbindungen. Zeitschrift für Naturforschung, A36, 1233–1238.

Hazen, R.M. (1977) Temperature, pressure and composition: Structurally analogous variables. Physics and Chemistry of Minerals, 1, 83–94.

Holm, J.L., and Kleppa, O.J. (1966) The thermodynamic properties of the aluminum silicates. American Mineralogist, 51, 1608–1622.

Hutton, D.R. (1969) Rotational properties of electron spin resonance spectra. Journal of Physics, C 2, 673–679.

Landry, R.J., Fourmer, J.T., and Young, C.G. (1967) Electron spin resonance and optical absorption studies of Cr^{3+} in a phosphate glass. Journal of Chemical Physics, 46, 1285–1290.

Le Marshall, J., Hutton, D.R., Troup, G.J., and Thyer, J.R.W. (1971) A paramagnetic resonance study of Cr^{3+} and Fe^{3+} in sillimanite. Physica Status Solidi, A5, 769–773.

Saalfeld, H., and Guse, W. (1981) Structure refinement of 3:2-mullite ($3Al_2O_3 \cdot 2SiO_2$). Neues Jahrbuch für Mineralogie Monatshefte, 145–150.

Schneider, H. (1986) Formation, properties, and high-temperature behaviour of mullite. Habilitationsschrift, Faculty of Chemistry, University of Münster, p. 1–148.

——— (1990) Transition metal distribution in mullite. Advances in Ceramics, in press.

Schneider, H., and Rager, H. (1986) Iron incorporation in mullite. Ceramics International, 12, 117–125.

Schneider, H., and Vasudevan, R. (1988) Structural deformation of manganese substituted mullites: X-ray line broadening and lattice parameter studies. Neues Jahrbuch für Mineralogie Monatshefte, 165–178.

Trömel, M. (1983) Empirische Beziehungen zu den Bindungslängen in Oxiden. 1. Die Nebengruppenelemente Titan bis Eisen. Acta Crystallographica, B 39, 664–669.

Wells, A.F. (1984) Structural inorganic chemistry (5th edition). Clarendon Press, Oxford.

Winter, J.K., and Ghose, S. (1979) Thermal expansion and high-temperature crystal chemistry of the Al_2SiO_5 polymorphs. American Mineralogist, 64, 573–586.

Manuscript received October 4, 1988
Manuscript accepted November 22, 1989